3D large-scale numerical model of open-pit lake slope stability-case study of Lake Most

Vincent Renaud, Marwan Al Heib, Jan Burda

3D large scale numerical model of open-pit lake slope stability – case study of Lake Most

Vincent Renaud [1], Marwan Al Heib [1] and Jan Burda [2]

[1] Institut national de l'environnement industriel et des risques (Ineris)-54042 Nancy- France
[2] Vyzkumny ustav pro hnede uhli (VUHU), tr. Budovatelu 2830/3, 434 01 Most - Czech Republic
* Corresponding author: vincent.renaud@ineris.fr; Tel.: +0033-3-5440-6632, ORCID ID: 0000-0003-0759-9995

Abstract

Almost all post exploitation open pit mines in the world are shaped as a final water reservoir. One of the main hazards is the slope stability of lake banks. To develop a reliability methodology for assessing the long-term stability of flooded open-pit lake, a back analysis was conducted using 2D and 3D large-scale numerical models of Lake Most, which is one of the largest mining lakes in Europe (Czech Republic). The large-scale numerical model was built, based on the site observations, large scale LiDAR data, in situ characterisation tests and statistical analysis of geotechnical data, on DTMs defining the complex geology of the site and on numerous piezometric levels to build the water table. Local and global safety factor (SF) were calculated using the strength reduction method. The results highlighted the reliability of the methodology to combine the geometric model with the geological model to create a large-scale numerical model, to identify local and potentially instable zones and to highlight the role of a weak contact layer. The calculation of 3D SF has shown a very good correlation between the lowest SF and the ground movement observations noted by the Czech authorities.

Keywords Open-pit lake Slope stability Strength reduction method Local and global safety factor Probability distribution.

1 INTRODUCTION

Almost all post exploitation open-pit mines in the world are generally shaped as a final reservoir intended to be filled with water (McCullough et al. 2020; Cala and Polak 2012; Johnstone 2018). In Europe, the creation of water reservoirs is the most common way of reclaiming post exploitation voids (Schultze et al. 2010, 2013; Oggeri et al., 2019, Redondo-Vega et al. 2021). These artificial lakes are currently (and in the future) reserved for economic and recreational purposes (Apostu et al. 2020). To ensure public safe use of these sites, it is necessary to assess the potential risk of instability of the lands taking into consideration the complexity and the history of the site (Wyllie and Mah 2017). The stability of pit lake slopes after flooding remains an area of uncertainty. Examples of geotechnical failures in slopes and banks of open-pit lakes are quite well documented, for example those at pit lake Pątnow (Geller et al. 2013), Zülpich Mitte and Lake Concordia near Nachterstedt (Vinzelberg and Dahmen 2014). The main reasons for these failures either were discovered following the incident or remain unknown. To understand the causal link behind this phenomenon it is necessary to perform a back-analysis of open-pit lakes conditions and compare the results to the original design conditions.

The study of the stability of natural and man-made slopes has progressed tremendously, employing advanced soil, rock mechanics and hydrology (Alejano et al. 2011; Bye and Bell 2001;

Hoek and Bray 1981; Wylie and Mah 2004; Caudal et al. 2017). Nonetheless, those studies concern generally a 2D or a simple 3D geometry. Nikolic et al. (2019) investigated the slope stability of an artificial lake to ensure the long-term safety using advance numerical modelling. However, several parameters can affect slope stability such as soil or rock strength, geological setting, topography, excavation geometry and water table position. The presence of water tables (and *a fortiori* a lake) in open-pit causes a change in pore water pressure (u), which is one of the parameters controlling the shear strength (τ) of geomaterials. The change in the pore water pressure causes a change in the effective stress (σ') in accordance with the famous relationship defined by Terzaghi (1925): $\sigma'=\sigma-u$. The Mohr-Coulomb failure criterion changes to $\tau = C+(\sigma-u)\tan\phi$ with effective stresses, where C is cohesion and ϕ the friction angle. This effect of pore pressure on the slope stability is the most important problem induced by water tables. In a rock mass, water pressure inside discontinuities reduces the shear strength (Atkinson 2001).

2 SAFETY FACTOR COMPUTATIONS

The slope safety is generally assessed with a global safety factor (SF) (the ratio of slip resistance forces to the shear forces). To compute a safety factor for a slope, 4 different numerical methods can be employed: the strength reduction method (Zienkiewicz et al. 1975; Matsui and San 1992; Dawson et al. 1999; Griffiths and Lane 1999; Soren et al. 2014), the limit analysis (statically admissible stress field and kinematically admissible deformation, Qiujing et al. 2017), the limit equilibrium method (an approximate method assuming the existence of a slip surface of simple shape, Bishop 1955; Jaeger 1971; Fredlund and Krahn 1977; Hoek and Bray 1981; Chen and Chameau 1982; Goodman 1989) and artificial neural networks (machine learning, Meng et al. 2021). Nowadays, the coupled analysis approach is receiving more attention in recent years because powerful numerical tools (2D and 3D finite element/difference analyses) are becoming easily available (Vanneschi et al. 2018).

Numerical modelling has become a prominent approach in assessing the slope stability of active and abandoned open-pit mines. Additionally, numerical modelling is used for studying the complex geometry and geotechnical aspects of open-pit slopes under flooding conditions (Steiakakis et al. 2016). The strength reduction method (SRM), based on the linear Mohr-Coulomb failure criterion is used for the safety factor calculations. A nonlinear failure criterion could also have been adopted (generalized Hoek-Brown) but it is more appropriate for rocks than for soils (Yongtao et al. 2021). This method is applied in safety factor calculations by progressively reducing the shear strength of the material to bring the slope to a state of limiting equilibrium. With the Mohr-Coulomb failure criterion (Zienkiewicz and Taylor 2000), the safety factor is defined by the following equations:

$$C^{trial} = \frac{C}{F^{trial}} \text{ and } \emptyset^{trial} = Arctan\left(\frac{tan\emptyset}{F^{trial}}\right) \quad (1)$$

Series of iterations are made using trial values of the factor to reduce the cohesion, and friction angle, until a slope failure occurs. The detection of the boundary between physical stability and instability is based on an objective criterion (the convergence threshold for example) that decides whether the system is in equilibrium or in a state of continuing motion. This method can be applied to essentially any material failure criterion: Mohr-Coulomb, Hoek and Brown, or the ubiquitous joint criterion.

The present work examines the slope stability of a deep open-pit lake: a case study from the Czech Republic (brown coal mining) is investigated and evaluated. The study focusses on the

back analysis and the prediction of the critical zones of the open-pit lake using a large scale (several km), non-linear soil-rock behaviour and non-homogenous terrains. The numerical modelling was used to analyse the stability of the slopes under the effect of a weak contact layer. The SF calculations presented in this study are based on the strength reduction method (simultaneous reduction of cohesion and frictional angle). Those 2 parameters are considered as random variables using different distributions (normal, log-normal and Birnbaum-Saunders distribution).

3 CASE STUDY: LAKE MOST

This study investigates the stability of a deep lake and of dumps in one of largest open-pit lakes in Europe, using a large-scale 3D numerical model and strength reduction method to calculate the local and global safety factor. This deep lake safety factor is crucial for the safety and the security of the area and for the valorisation of the open pit lake. The final destination of Lake Most is the creation of a leisure site. This section presents the data used for the modelling purpose based on deep historic investigation, in situ observations and laboratory and in situ investigation for constructing the numerical model.

3.1 Site description

Lake Most is one of the largest open-pit lakes in Europe, located below the Hnevin hill in the North-West of Czech Republic (Fig. 1), corresponding to the central part of the Most Basin (the former North Bohemian Brown Coal Basin), which is a geomorphological whole in the Podkrusnohorsky region of the Krusne Mountains. This lake was formed on the site of the former royal town of Most. From the 18th century onwards, mining operations took place and changed the basin's original flat relief. At first, the coal underground extraction was carried out in connection with the industrial development of the Most region. After 1948, there was a rapid development of large open-cast coal mines, resulting in the demolition of the historical Most town in 1965–1987 and the construction of a new town. Coal mining activity was definitely stopped on the 24th of August 1999. Lake Most is defined as the area between the Hnevin and Spicak hills (both 399 m ASL) with the flooded residual pit surrounded by Ruzodoslka dump in the south, the Celio landfill in the north, further by the Venuse ash dump and heaped body of the Strimice dump in the east and the coal pillar Kopisty and Cheza site with adjacent K1-K4 ash dumps in the west. The elevation around Lake Most is graphically represented by a hypsographic curve (Fig. 1).

Flooding was started on October 2008 where the banks and adjacent slopes are made of dump soil. The southern slopes of the lake generally face north with a slope of 5 - 10^{o}. The slope resembles a slightly inclined platforms (up to 2^{o}) with two visible berms 10-15 m high. The northern slopes of the residual pit are formed by the earthen body of the Konobrze dump, which fulfils a stabilizing and sealing function. The body of the dump was formed between 1997-1999 in three dump berms. Before flooding, the lake had an area of 21.6 ha and a depth of 21.12 m. In the first half of 2012, the water surface level reached 198.03 m ASL, which corresponds to an area of 297.91 ha with a total water volume of 69.809 million m^3. In May 2014, Lake Most was flooded to the final permanent water level of 199.00 m ASL. The water level fluctuates in the range of ± 60 cm (Zizka and Burda 2021).

The most frequent slope instability observed (Fig. 2) during the construction and the flooding phases are landslides. The most recent landslides were found in the northern slopes and in the Konobrze dump area, the separating areas form mostly at 220 - 250 m ASL. The depth of the observed ground movements varies usually between 5 and 20 m. Several old large landslides are currently “buried” (meaning covered) by dump material.

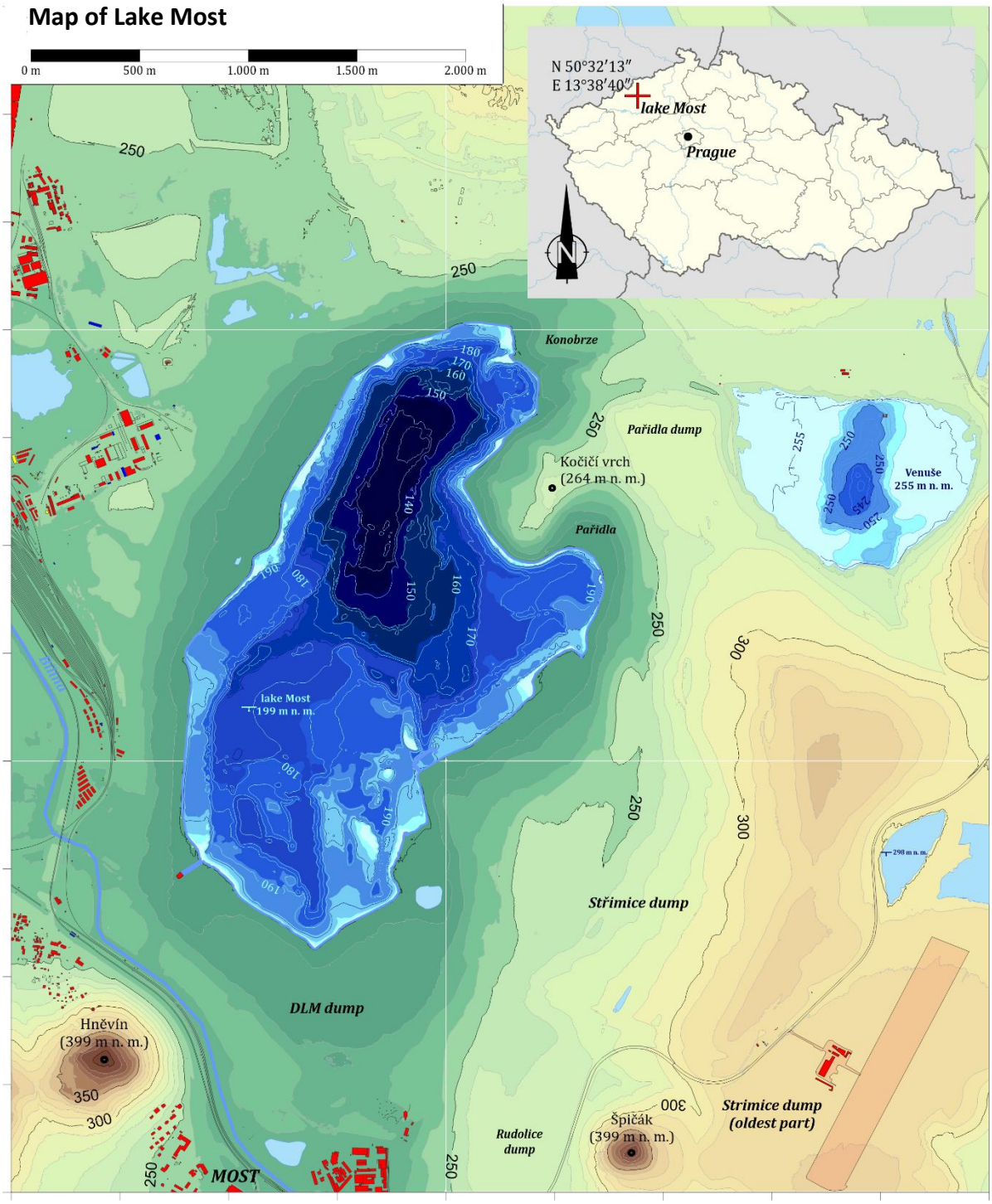

Fig. 1 Localization of Lake Most – Czech Republic

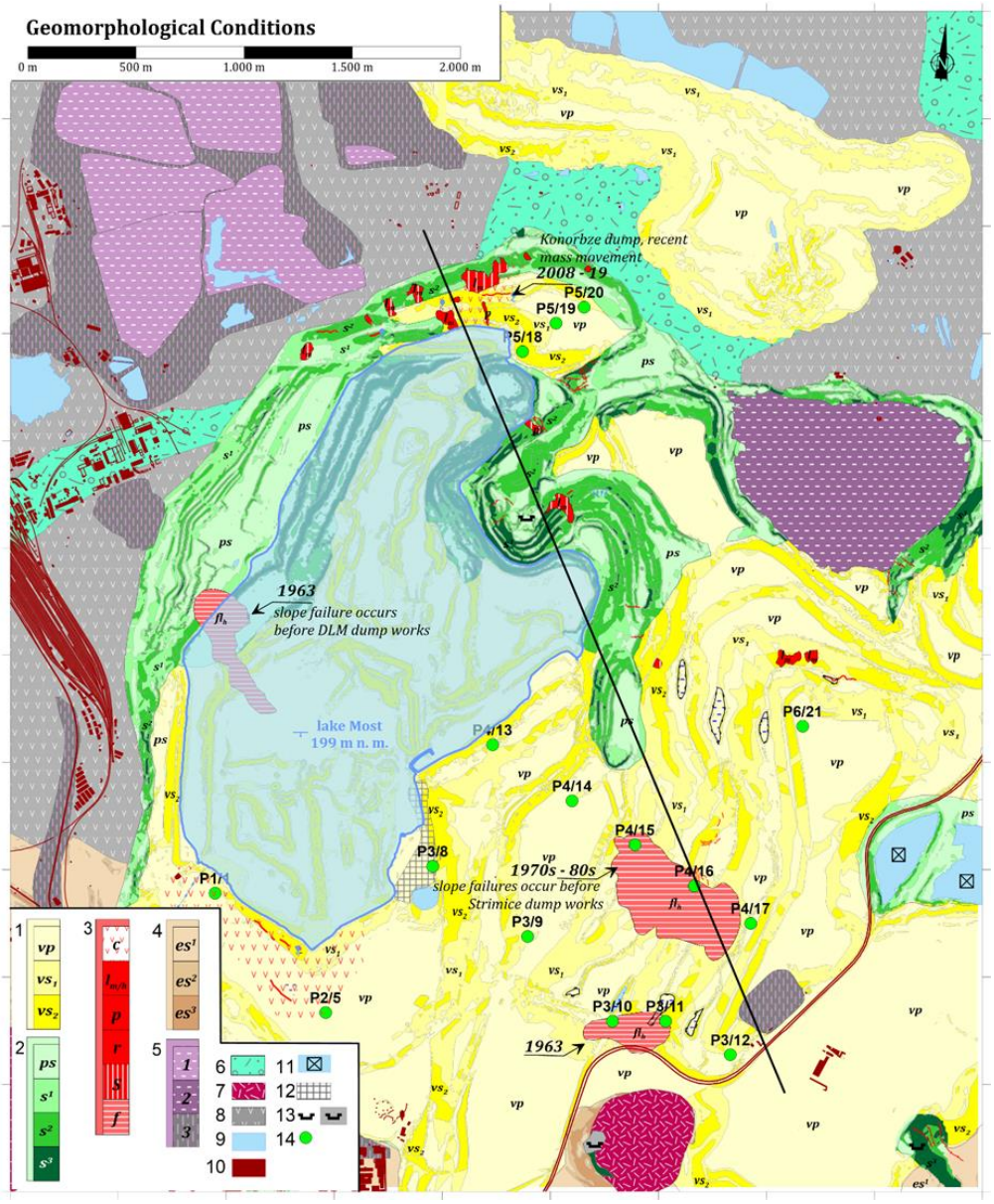

Fig. 2 Localisation of CPT boreholes around Lake Most, D cross-section (black line) and localisation and dates of ground movements. **Legend : 1 – Dump slopes: vp – plains (0-2°), vs1 – slopes (2 – 5°), vs2 – slopes (over 5°); 2 – Open-pit slopes: ps – plains (0-2°), s1 – slopes (2 – 5°), s2 – slopes (5 – 15°), s3 – slopes (over 15°) ; 3 – Slope deformations: c – creep, lm / lh – landslide shallow/deep, p – earthflows and mudflows, r – rockfalls, s – stabilized landslides, f – buried landslides; 4 - Fluvial Erosional Landforms: es1 – Erosional slopes (under 5°), es2 – Erosional slopes (5 – 10°), es3 – Erosional slopes (over 15°) ; 5 – Sludge ponds: 1 – abandoned, 2 – active, 3 - landfill; 6 – Proluvial plains (original surface); 7 – Neovulcanic elevations (original surface); 8 - Subsidence basin after deep mining; 9 – Water area ; 10 – Buildings and infrastructure; 11 – Flooded quarries; 12 – Stone wall; 13 – Stone mines/stone heap; 14 – Position of CPT boreholes**

3.2 Geological data

The Most Basin is a relic of the Tertiary sedimentary basin, filled with sedimentary material. It originated mainly in the Miocene period. Between 22 and 17 million years ago, up to 500 m of clay, sand and organic matter piled up in this basin. A brown coal seam formed in most of the basin area, from peat layers deposited in the Tertiary marsh. In places where rivers flowed into the marsh, supplying the marsh with water, the peat sedimentation was suppressed by clay

and sand deposition. In these places, the seam is completely replaced by river or delta sediments or split into several benches. Geological studies of the Most basin have identified fourteen geologic formations, not at all of them tabular (Fig. 3). Also, thousands of boreholes (excavated between 1867 and 2018) have been used to build a DEM (Digital Elevation Model) of the interfaces of the different formations. The simplified geological cross-section of the different layers is represented in Fig. 3. The recent layers (from the Quaternary to the Miocene) are divided into 2 main groups. The first one corresponds to 3 coal seams and a clay layer, sandy clays (PJIL layer), 3 plastic clays layers (JIL1, JIL2 and JIL3) and Quaternary gravel and the second group corresponding to anthropogenic layers (dump materials) and concerns 4 geological layers (NS, TV1, TV2, contact layer). A contact layer is potentially located at the base of the dump and has the weakest strength of all layers (see Fig. 11). These soils are permanently in contact with water flowing on the ground. In places where the thickness of dump soils reaches 80 - 100 m, their structure could have collapsed. Due to its very weak properties, the contact layer can have a major influence on slope stability (Mikroutsikos et al. 2021).

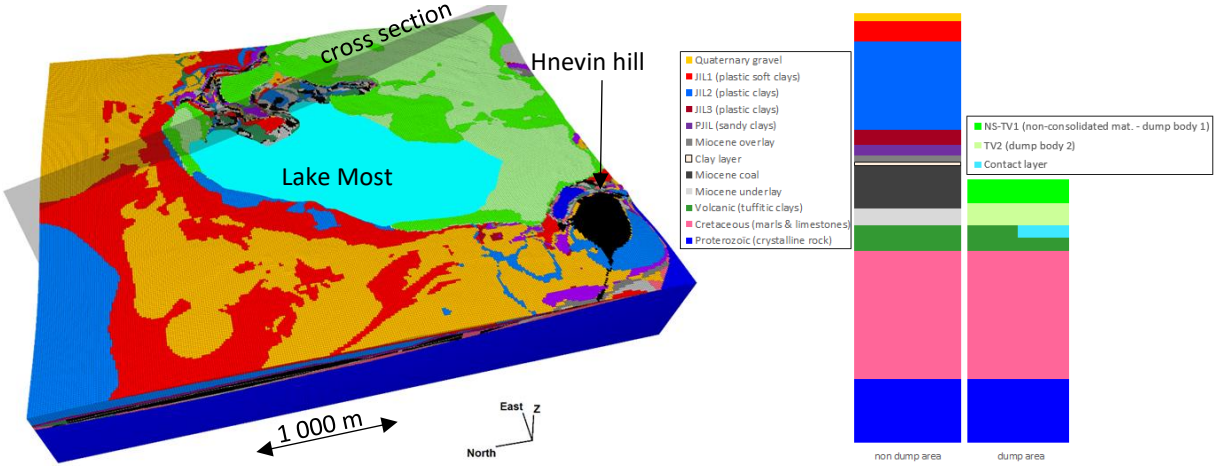

Fig. 3 Main geotechnical units: geological layers and anthropogenic layers (dump area, with or without contact layer) represented with a homogeneous mesh

3.3 Geotechnical data

3.3.1 Non-dump area

The different geotechnical data were summarized based on laboratory and in situ characterization. Some geomechanical parameters (cohesion and friction angle) are known, in particular for the formations of the surface up to the mined coal seams (JIL1, JIL2, JIL3, PJIL, MO, MC, MU, Table 1). Reasonable data based on the geology description and the equivalent soils, was compiled to replace the missing data. Table 1 presents the different geotechnical parameters for 11 layers. They are used in the numerical model presenting the characterization of the equivalent parameters of the rockmass. It should be noted that the Cretaceous and Proterozoic layers are assumed to exhibit an elastic behaviour, while the other layers exhibit a plastic behaviour.

Geotech-nical layer	Description	γ_{unsat} (kN/m^3)	γ_{sat} (kN/m^3)	C (kPa)	ϕ (°)	ψ (°) (0 ; ϕ/3)	E (MPa)	ν
Q	Quaternary gravel	19	21	50	20	0	40	0.35
JIL1	Plastic soft clay	20	22	**57**	**9.5**	0	70	0.35
JIL2	Plastic clay	20	22	**93**	**17**	0	70	0.35
JIL3	Plastic clay	17	18	**72**	**13.8**	4.6	60	0.35
PJIL	Sandy clay	18	20	**15**	**30**	10	100	0.35
MO	Miocene overlay	15	18	**50**	**35**	11.7	120	0.3
MC	Miocene coal							
MU	Miocene underlay							
Clay	Clay layers inside coal seam	17	18	93	18	6	60	0.35
TUF	Tuffitic clays, weathered basalt, tuff	21	23	500	25	8.3	3000	0.35
Cretaceous	Marls, clayey marl and limestone	23	25	elastic			5000	0.35
Proterozoïc	Crystalline rock	23	25	elastic			20,000	0.3

γ_{unsat}: unsaturated density, γ_{sat}: Saturated density, C: cohesion, ϕ: friction angle, ψ: dilatancy angle, E: Young modulus, ν: Poisson ration

Table 1 Geomechanical parameters of geological layers; in bold measured data, in regular: suggested data

3.3.2 Dump area

In the dump material, a penetrometric measurement campaign was carried out on the foot of the dumps around Lake Most (Fig. 2) using 23 boreholes corresponding in total to 9538 CPT (Cone Penetration Test) measurements. The depth of the boreholes varies between 10 m and 100 m. The dump thickness varies between 30 m and 120 m. The CPT information was used to determine both the position of interfaces between geologic layers as well as the values of the geomechanical parameters. The initial results of the 9538 CPT are: pore pressure (u_2), sleeve friction (f_s), depth, cone resistance (q_c), corrected cone resistance (q_t), soil weight (γ), density (ρ), pore water pressure (u), total stress (σ_v) and Young's modulus (E). The cohesion (C) and the friction angle (ϕ) was estimated based on the CPT results. Three empirical relationships (Robertson and Campanella 1983; Kulhawy and Mayne 1990; Mayne 2006) are suggested for computing the friction angle. These relationships, however, cannot determine the cohesion and their validity is limited for sands or fine-grained soils. Two equations are proposed by Motaghedi and Eslami (2014) allowing the calculation of the two soil parameters: C and ϕ.

$$\begin{cases} u_2+\gamma B\tan\phi+(\sigma_v-u)N_q+\gamma BN_q\tan^2\phi+C\dfrac{N_q-1}{\tan\phi}=q_t \\ C=f_s-0.000789(1-\sin\phi)(\sigma_v-u)\tan\dfrac{2\phi}{3}\left(\dfrac{q_t-\dfrac{\sigma_v}{3}(1+2(1-\sin\phi))}{\dfrac{\sigma_v-u}{3}(1+2(1-\sin\phi))}\right)^{1.44} \end{cases} \quad (2),\ (3)$$

$$\text{with the bearing capacity factor } N_q=\frac{(\sin\phi+1)^2}{\cos\phi}\exp\left[\left(0.0061\frac{q_t}{P_a}+2.4\right)\tan\phi\right] \quad (4)$$

The *C* in equation (2), is itself expressed algebraically in equation (3), thus yielding a third equation with a single unknown *(ϕ).* This equation can only be solved numerically (e.g. with the Mathematica solver). But since this function of ϕ is monotonic, increasing and differentiable, the resolution can be quickly achieved with the Newton-Raphson method which can be easily implemented in MS Excel: $\phi_{i+1} = \phi_i - \frac{f(\phi_i)}{f'(\phi_i)}$. Indeed, in less than 10 iterations, the friction angle is calculated to a very good accuracy. Depending on the case, we initialize ϕ_0 with 0.6 or 0.9 rad (34° or 52°) to obtain a quadratic convergence. Thanks to this calculation, the cohesion and the friction angle were obtained for each CPT measurement. Furthermore, the geomechanical parameters were used to identify the different soil layers of the dumps. The dump is composed of three main layers (NS, TV1 and TV2) and the contact layer. The position of the contact layer can be obtained using only two CPT (P3_9 and P4_14), because their depth is greater than the estimated thickness of the dump body.

It was not possible to distinguish the interface between the NS and TV1 layers (which had to be between 10 m and 20 m deep corresponding to the dump thickness). That is why, from a mechanical point of view, these 2 layers have been combined into one (NS-TV1).

Fig. 4 presents an example of the distribution as a function of depth of the geomechanical parameters. To discriminate the NS-TV1 layer and TV2 layer, several approaches exist. Some of them are based on the classification of soil types (Soil Behaviour Type charts proposed by Robertson et al. 1986; Robertson 1990, 2010; Schneider et al. 2008). The problem with the soil classification is that 2 types of soils can have the same cohesion and friction angle. This is in part because this classification is based on fewer measured parameters than the calculation of *C* and ϕ. The approach that was used here is based on a statistical analysis. For that, the geotechnical characterization is statistically analysed for the 23 cohesion profiles and more precisely to check from what depth the coefficient of determination (r^2, between depth and cohesion) decreases. Indeed, the more data there is that follows a linear trend, the more that r^2 increases. To get a significant decrease of r^2 while the population is high (n>200), there must be a sudden change in trend. These significant variations in r^2 could be easily observed for depths very often greater than 20 m (Fig. 4). In this analysis, the cohesion was retained that positions the interface between NS-TV1 and TV2. The interface between NS-TV1 and TV2 could be detected statistically for 20 profiles out of the 23. The analysis of Table 2 shows the contribution of unit division: the coefficients of variation (COVs) of *C* and ϕ are significantly lower when the measurements are separated into 2 geotechnical units rather than considering the whole profiles (the measurements belong to a single layer).

The Czech territory is divided into 6 seismic zones (European EN 1998-1 standard). The value of the maximum reference acceleration for the area including Lake Most is equal to 0.39 m/s² or 0.04 g which is a low value with regard compared to the seismicity in other European countries. The maximum reference acceleration of 0.04 g could correspond to an equivalent increase in the slopes of approximately 2° for a short time. The effect would therefore be limited and has not been considered in this study.

	Cohesion *C*	Friction angle (ϕ)
Whole profile	50% - 109 %	19 % - 56 %
NS-TV1 unit	20 % - 72%	12 % - 29 %
TV2 unit	16 % - 57 %	7% - 33 %

Table 2 Variation interval of coefficient of variation (*C* and ϕ) of the 23 CPT profiles

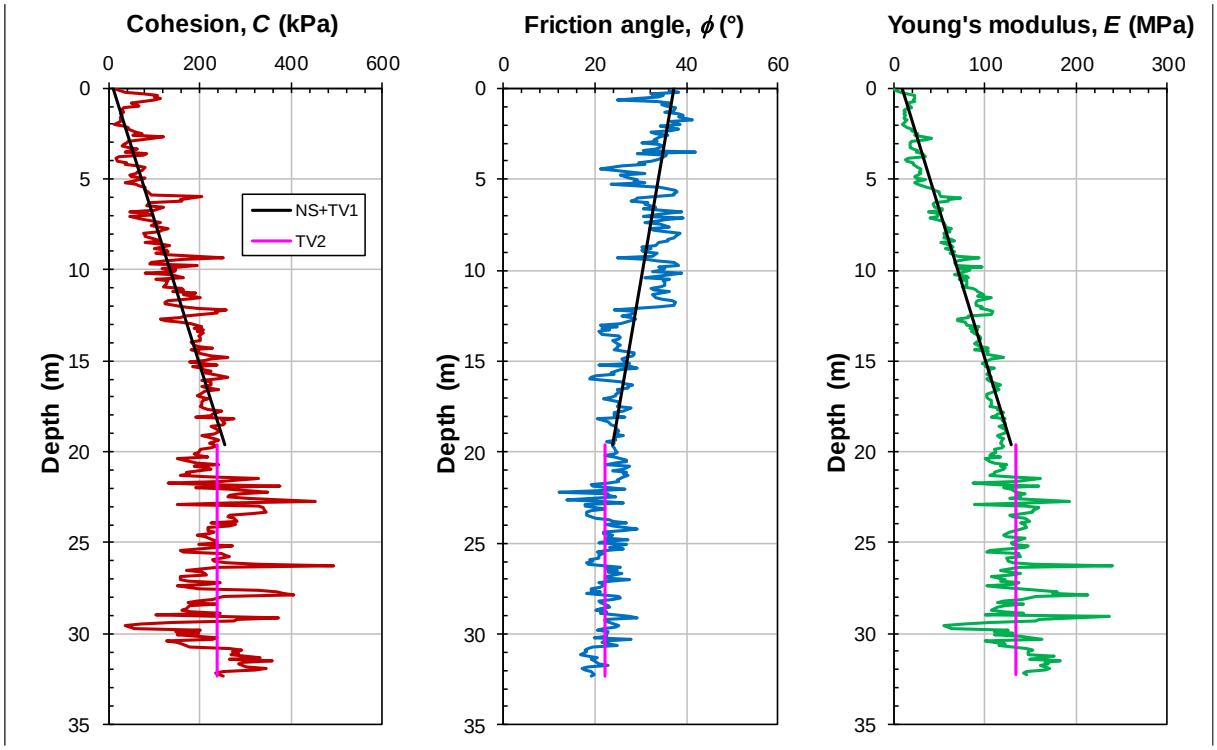

Fig. 4 Example of geomechanical parameters distribution for profile P1_2

Fig. 5 presents the parameters of the NS-TV1 layer along the depth of profiles. This allows noise to be removed from data that would otherwise be unusable without statistical processing. In this way, the means and the minimum and maximum bounds of cohesion, friction angle and Young's modulus for each dump layer were calculated for all the 23 profiles.

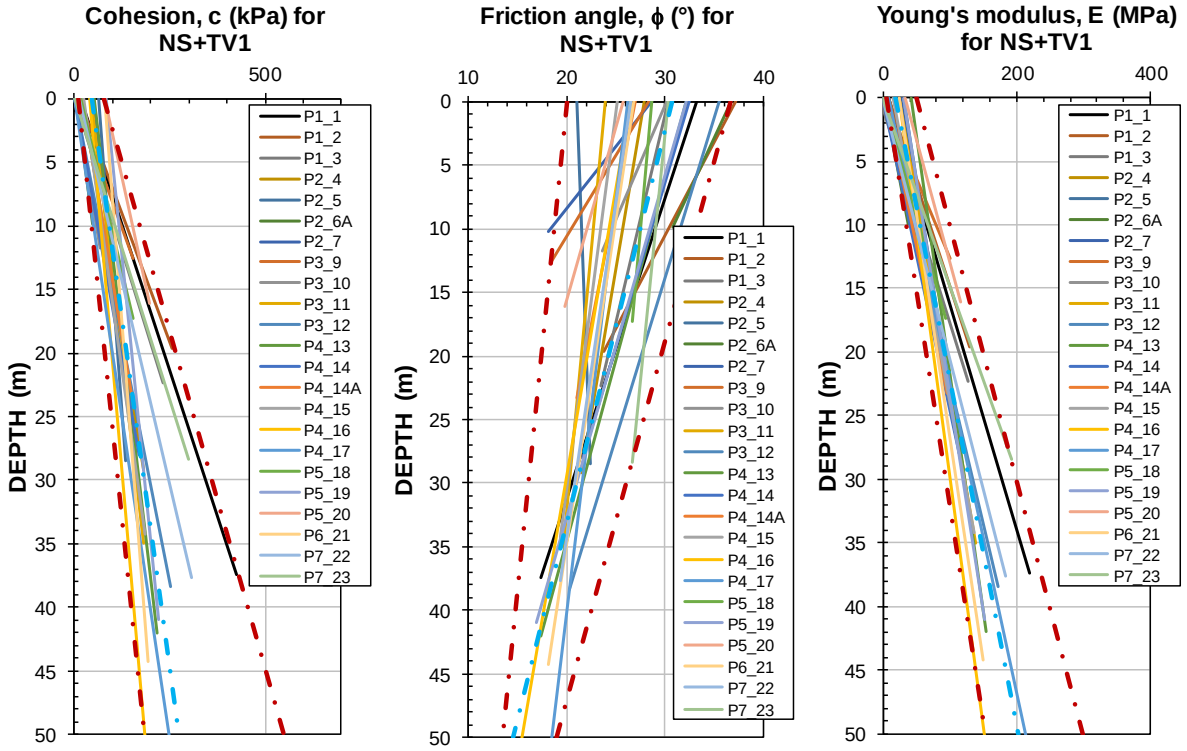

Fig. 5 Linear variation of cohesion, friction angle and Young's modulus for 23 CPT profiles for NS-TV1 layer; minimum and maximum limits in red and mean value in cyan

Analysis of the measurements for each profile showed a dependency of the values of *C*, ϕ and *E* with depth (vertically) for the NS-TV1 layer unlike the measurements for the underlying TV2 layer. This can be explained by a greater consolidation of the lower layers which tends to limit the variability of mechanical properties. Therefore, the minimum and maximum bounds of cohesions, friction angles and Young's modulus are taken to be constant for TV2 while they vary linearly for NS-TV1. The analysis of the CPT measurements according to the spatial position of the boreholes (x, y) showed that no spatial dependency of the geotechnical parameters is observed. For the NS-TV1 layer, it is not surprising that the cohesion and Young's modulus increase with depth (Fig. 5) while the friction angle decreases with depth. This decrease has less effect than the increase in cohesion. The decrease of ϕ concomitant with the increase of *C* is a known phenomenon, verified by analysing the correlation between these 2 parameters (Theocharis et al. 2021). The calculation of the correlation coefficient *r* shows, unsurprisingly, that the anti-correlation values correspond to the values that can be found in the literature (Theocharis et al. 2021). The value of *r* varies between -0.11 and -0.83 with a mean value of -0.37 (Fig. 6).

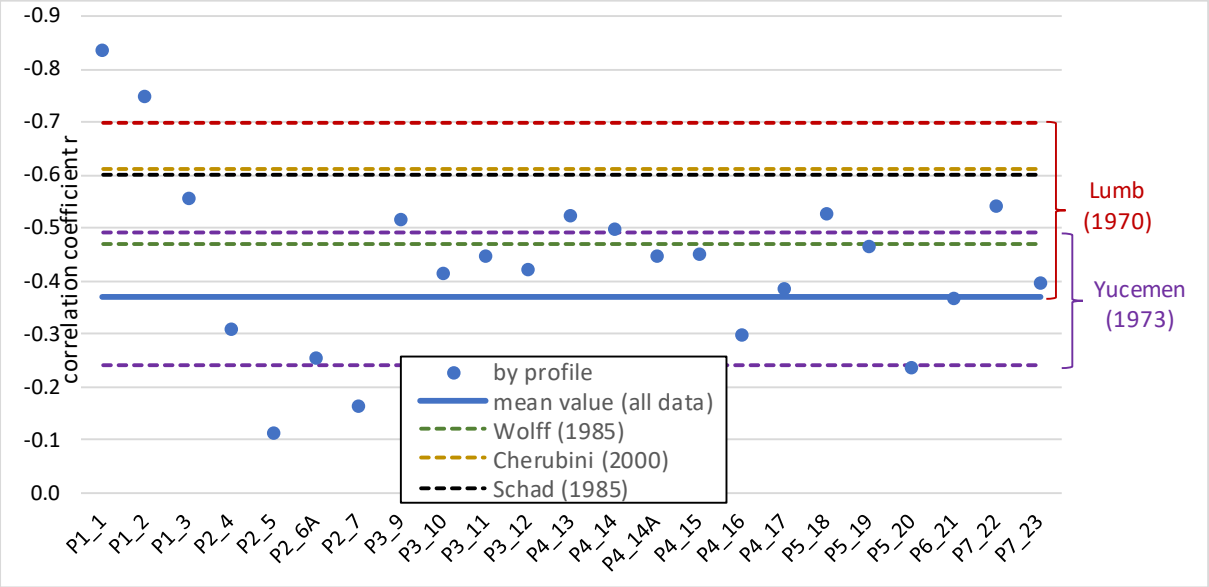

Fig. 6 Correlation coefficient between *C* and ϕ by profile and for the whole data set, comparison with literature values

3.4 Geometrical, geological and mesh generation

The model dimensions are based on the lake data. The maximum depth of the lake being 75 m, with the highest hill in the immediate vicinity of the lake having a height of 70 m, relative to the surface of the lake. Based on the state of the art and to avoid the influence of the boundaries on the numerical results, the vertical boundary of the model should be positioned (Merrien-Soukatchoff and Omraci 2000) at least, 5 times 70+75 m (i.e. 725 m). The horizontal boundaries of the 3D model were positioned at 1 300 m, 1 050 m, 900 m and 1 160 m respectively from the north, east, south and west shores of Lake Most (Fig. 8).

To construct the topography of the 3D model and the soil layers, different techniques were used (Gallwey et al. 2019). The topography of the 3D model results from the combination of 3 different point clouds: bathymetry, laser scan and cadastral mapping. The model integrates the areas of ground movement previously identified and considers the valleys and the hills located in the zone of interest.

To avoid too many meshes and leading to prohibitive calculation times, an area of interest was defined (Fig. 8). To achieve a compromise between huge extension of the model and detail on evolution of different failure modes observed along slopes, a mesh sensitivity study was carried out on a 2D model with the same slope characteristics as the shores of Lake Most. The analysis of these computations showed that the calculation of the FS became sufficiently stable for a mesh less than or equal to 5 m. This mesh size is compatible with the dimensions of the ground movement zones. Furthermore, because the spatial distribution of the boreholes is not homogeneous and does not always extend to the limits of the model, it was necessary to interpolate and extrapolate the position of these interfaces. As these are numerous (14), they sometimes have intersections, thus making it impossible to mesh the volume automatically (Fig. 3). Consequentially, only the interface between the Proterozoic and the Cretaceous was considered in the geometrical model. For other formations, the mesh is not conditioned by the position of their interfaces.

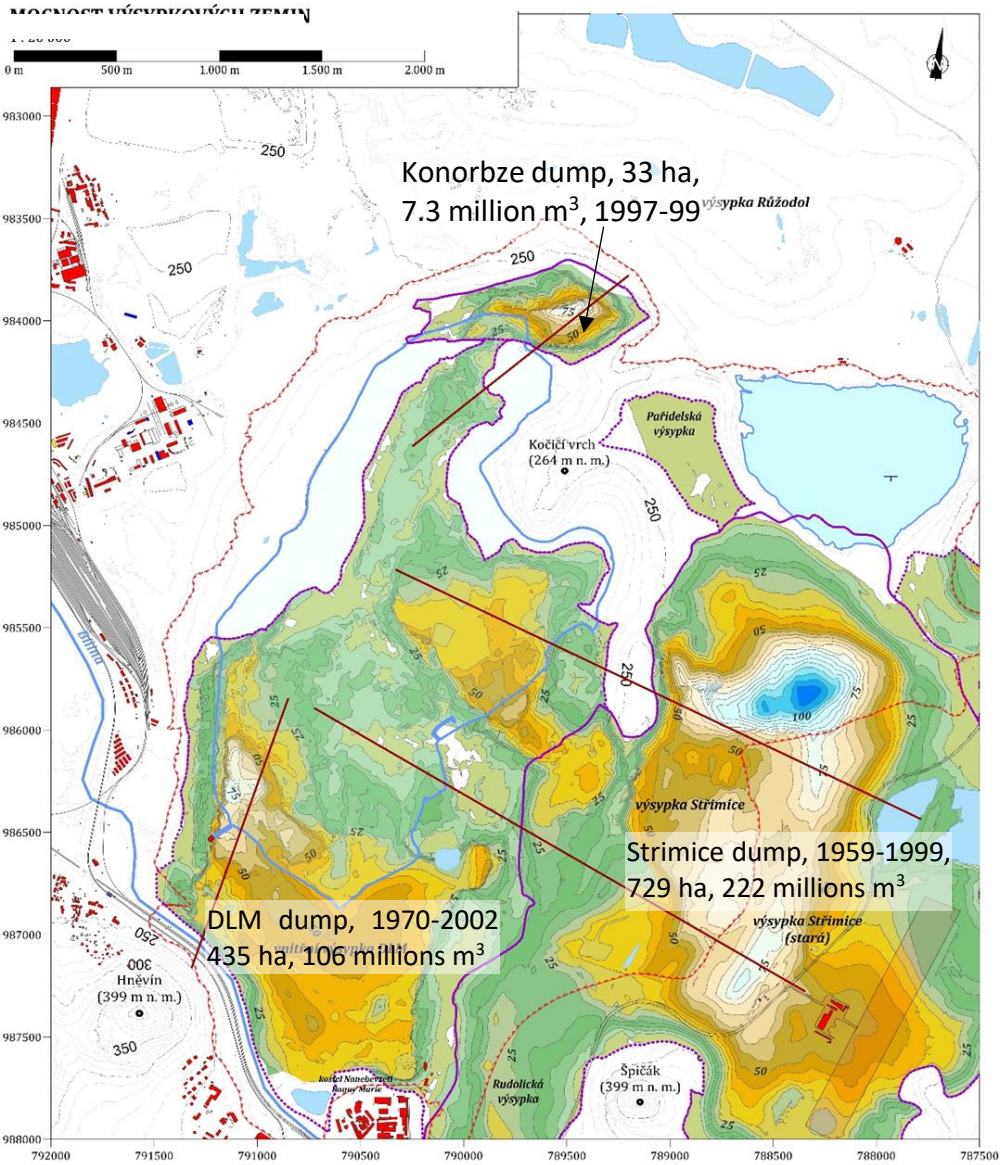

Fig. 7 Iso-thickness of dump body (Lake Most), purple lines corresponding to the dump limits

The DTMs (digital terrain model) do not allow describing the thicknesses and depths of the layers, because these parameters are too variable over the model volume. Thus, some DTMs have been built using existing DTMs or from specific data. The bases of the dumps were rebuilt from contours of iso-thickness (Fig. 7); the interface between TV1 and TV2 units is positioned based on the CPT analysis. The contact layer has been arbitrarily shifted 10 m below the base dump, and the clay layer (thickness of 5 m) has been inserted in the middle of the Miocene coal layer.

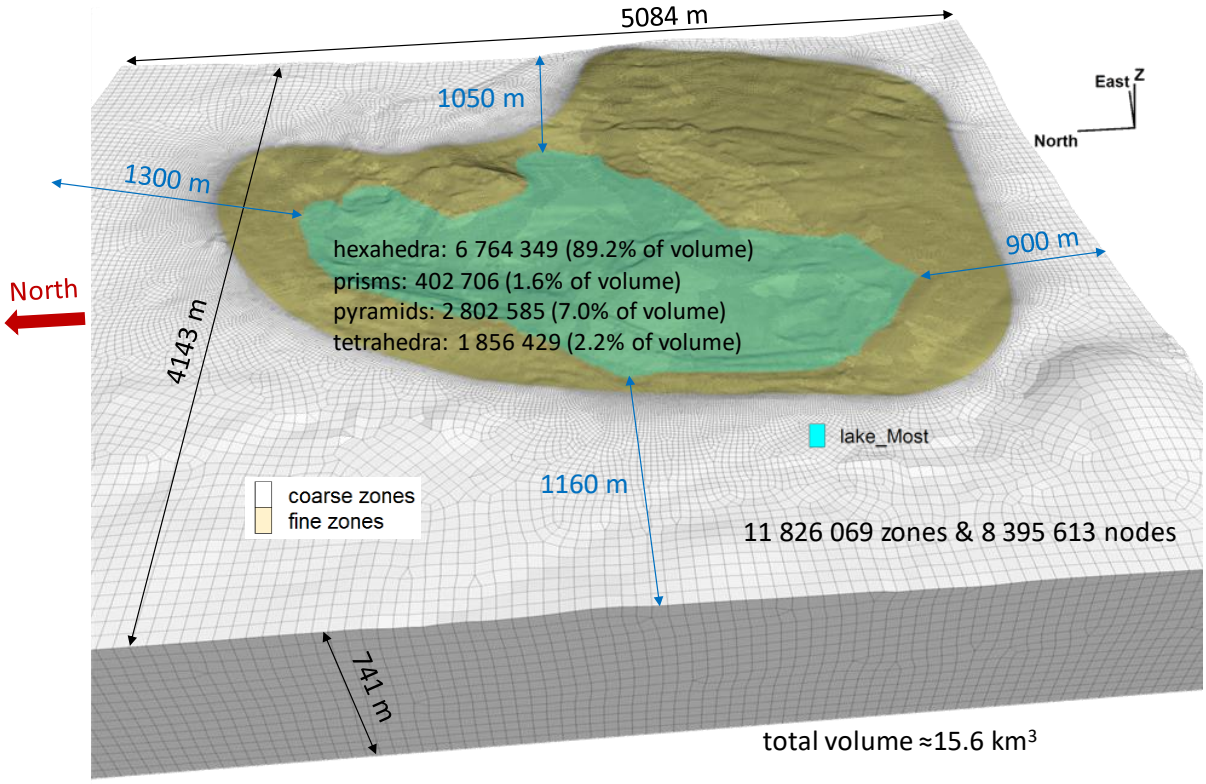

Fig. 8 Geometry and position of boundary conditions for the 3D model (Lake Most)

3.5 Modelling the heterogenous materials of dumps

The analysis of geomechanical parameters of the dump layers reflect the heterogeneity of the soils. In order to take this heterogeneity into account, a statistical distribution applied using different distribution laws: normal, log-normal and Birnbaum-Saunders distribution. The results of this statistical analysis are reported (Table 3). Note that the lognormal distribution is the one that best represents variations in cohesions and Young's modulus. The same is true for the friction angle except for the TV2 layer which correlates better with a Birnbaum-Saunders distribution. On the other hand, the normal distribution is well adapted to represent the spatial distribution of the density masses in the 23 CPT profiles. The probability density function of the Birnbaum-Saunders distribution is:

$$pdf = \frac{\sqrt{\frac{x}{\beta}} + \sqrt{\frac{\beta}{x}}}{2\sqrt{2\pi}\gamma x} e^{-\frac{\frac{x}{\beta}+\frac{\beta}{x}-2}{2\gamma^2}} \text{ with } \beta = \frac{\mu}{3}\left(4-\sqrt{3c^2+1}\right),\ \gamma = \sqrt{\frac{2\left(c^2-1+\sqrt{3c^2+1}\right)}{5-c^2}} \text{ and } c = COV = \frac{\sigma}{\mu} < \sqrt{5} \quad (5)$$

with β the median and γ the shape parameter

Fig. 9 shows how cohesion is spatially distributed in the NS-TV1 and TV2 layer (above the contact layer, in blue) in the 2D model. The friction angle, the cohesion and the Young's modulus distributions were adopted in the 2D and 3D numerical modelling.

Table 3 also represents the characteristics of the contact layer, the interface between dump and rock mass, with a low cohesion and friction angle.

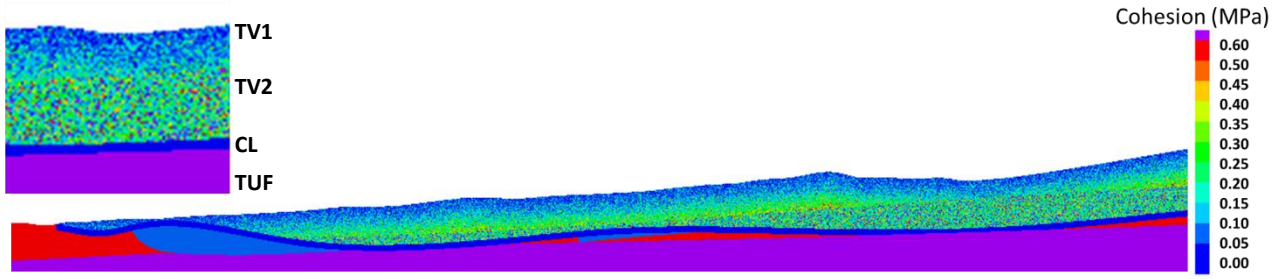

Fig. 9 Distribution of the cohesion in the NS-TV1 and TV2 layers

Geomechanical parameter		Dump layers		
		NS-TV1	TV2	CL
unsaturated density	γ_{unsat} (kN/m^3)	18.0	19.2	17.0
Saturated density	γ_{sat} (kN/m^3)	19.0	20.2	20.0
cohesion	*C* (kPa)	μ: 4.59 *d*+46.15 min: 3.5 *d*+10 LN dist ∫ [0.6, 650]: μ_{LN}=0.0324 *d*+4.034 σ_{LN}=-0.0063 *d*+0.598	mean: 247.4 min: 4 *d*-60 LN dist ∫ [6, 1098]: μ_{LN}=5.31 σ_{LN}=0.626	6.0
friction	ϕ (°)	μ: -0.323 *d*+30.69 min: -0.13 *d*+20 LN dist ∫ [7, 44]: μ_{LN}=-0.241 *d*+28.73 σ_{LN}=-0.071 *d*+6.074	μ: 22.7 min: 16.8 BS dist ∫ [8.2, 38.6]: β=22.019 γ=0.244	6.0
dilatancy angle	ψ (°)	0	7.6	2.0
Young's modulus	*E* (MPa)	μ: 3.67 *d*+18.51 min: 2.96 *d*+5 LN dist ∫ [1, 354] μ_{LN}=0.037 *d*+3.577 σ_{LN}=-0.004 *d*+0.377	μ: 193.9 min: 3.6 *d*-52 LN dist ∫ [29.6, 636.5] μ_{LN}=3.855 *d*+32.046 σ_{LN}=0.6195 *d*+28.295	70
Poisson's ratio	ν	0.35	0.35	0.3

N: Normal law, LN: Log-normal law, BS: Birnbaum-Saunders law, d: depth, μ: mean, CL: contact layer

Table 3 Statistical geomechanical properties of dump layers

3.6 Hydraulic data

The position of the water table obtained using hydromechanical equilibrium is as uncertain as the values of hydraulic parameters such as permeability. Fortunately, the Lake Most site is very well instrumented: the piezometric heights of the water table have been recorded for 93 wells since 2014. The water table DTM has been built from piezometric data and lake surfaces. The analysis of 93 wells yielded the corresponding piezometric water levels. But as can be seen in Fig. 10, these wells are essentially distributed on the east and west banks of the lake. Points were therefore arbitrarily added (in yellow in Fig. 10 = extrapolations) on the edges of the area to be modelled. These virtual wells are assumed to have the same piezometric depths as the neighbouring wells. It is essential to ensure that the water table not extend above the topography in any location (this may occur with extrapolations made for undersampled areas). Indeed, there is the risk obtaining tensile elements ($\sigma'_{zz}>0$) near the topographic surface because the pore pressure will have been overestimated. These possibly tensile elements would thus incorporate artificially amplified displacements when calculating the safety factor which would itself end up being too low as a result.

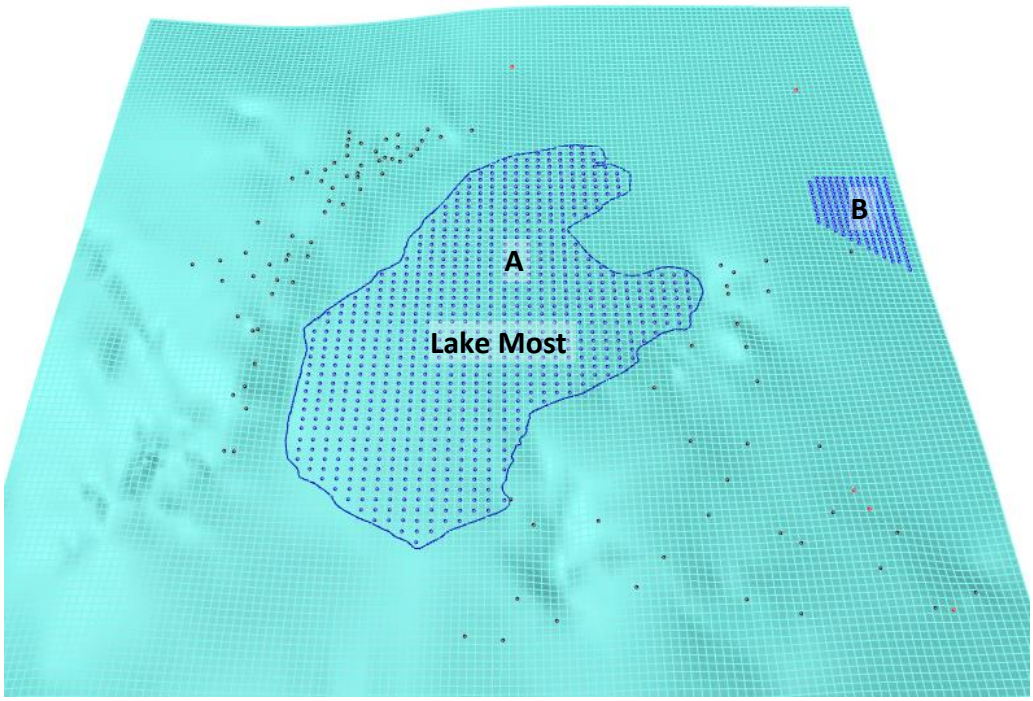

Fig. 10 Water table surface of Lake Most based on piezometric measurements

The volume of the lake has stabilized since May 2014 and the piezometric levels show a high position of the water table (8.9 m average depth in the area of interest). Under these conditions, it is reasonable to assume that a quasi-stationary hydraulic regime has been reached, and that the calculation of seepage flows can be neglected. The calculations presented in this paper therefore do not explicitly consider the effects of permeability, which can be a favourable factor for the slope stability if horizontal permeability is larger than the vertical one (Qiujing et al. 2017). The influence of the flooding speed (Lazar et al. 2020) on the slope stability has not been studied either.

3.7 Models' description

3.7.1 Safety factor calculation approaches

Usually, use of the strength reduction method produces one global minimum stability state per simulation. However, along a complex slope profile, it is interesting to be able to compute multiple minimum states. A local safety factor (LSF) method has been proposed by Yang et al. (2016) to evaluate the stability of different sections of a landslide. Based on 3D modelling, the LSF is defined as the ratio of the shear strength of the soil at an element on the slip zone to the shear stress parallel to the sliding direction of that element. Another way to determine several local stability states with the strength reduction method is to exclude different regions of the slope when performing the strength reduction calculation. This technique is based on the velocity magnitude of each node of mesh which has been stored for each global SF tested. By comparing the velocity data at a node against a limiting velocity, one can determine the greatest computed SF that resulted in that specific node being stable.

The advantage of accessing the local minima of the SF is to be able to assess the stability gap with adjacent areas. Indeed, a high SF gradient makes it possible to restrict the dimensions of the unstable zone while weak gradients (or opposite signs) testify rather to several unstable zones with large dimensions. These SF calculations are long: 2 weeks without the contact layer and 3 weeks for the calculation with the contact layer. These calculation times consider an optimization performed by increasing the criterion for stopping the calculations (ratio of unbalanced forces) compared to that used for the 2 calculations of the global SF. This optimization was validated by verifying that the overall minima are the same for calculations with or without SF isovalues.

3.7.2 2D models

Based on the geomorphology, 3D geometric and geological model, of the site and the ground movements, a vertical section was studied (Figs. 2, 11). This NNW-SSE cross section passes through the terrain movement zones north and southeast of the site. This section does not cut the lake into 2 equal parts but passes through the sectors with greater terrain slopes (up to 25°).

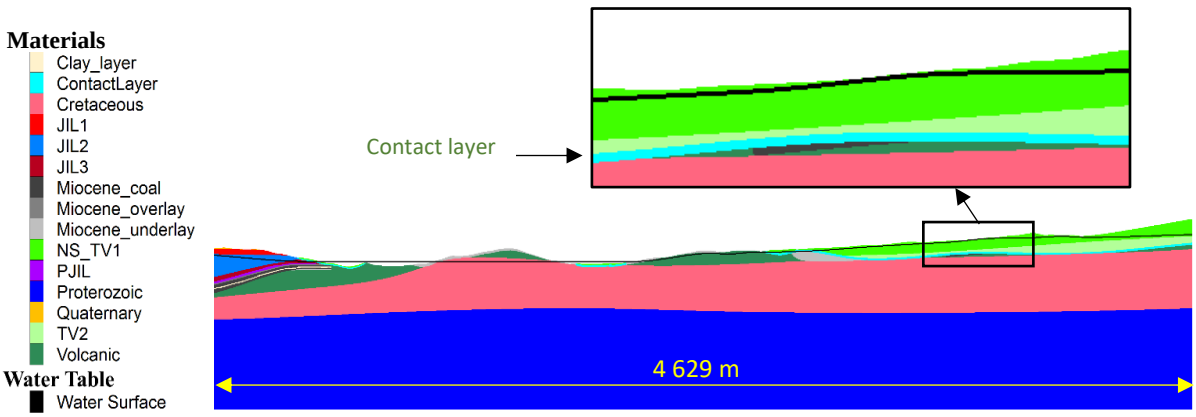

Fig. 11 2D numerical model corresponding to NNW-SSE cross section (see Fig. 2)

The mesh was performed using Griddle for Flac3D (Itasca 2019). The mesh fineness varies between 17 m and 1.7 m, which corresponds to 183,807 mostly hexahedral elements. The fineness of the mesh near the surface and in layers with low geomechanical characteristics ensures good accuracy of the safety factor calculation.

Six calculation scenarios were made to estimate the safety factor of the Most site in its current situation (Table 4). These 6 calculations were performed using the scenarios based on the geomechanical properties of the dump layers NS-TV1 and TV2 (mean values, minimum bounds or statistical distribution, see Table 3) and the presence or not of the contact layer at the bottom of the dump bodies.

Scenario n°	Set of properties	Presence of contact layer
1	mean values	no
2	distributions	no
3	minimum values	no
4	mean values	yes
5	distributions	yes
6	minimum values	yes

Table 4 Scenarios of calculation for NNW-SSE 2D cross section, current situation

3.7.3 3D model

Fig. 8 represents the geomechanical 3D model. The DTM surfaces generated with Rhino therefore result more from extrapolation than interpolation. It is then likely that the geological layers do not correspond to reality near the boundaries of the model. This is particularly the case for the Southwest corner (near Hnevin hill, Fig. 12 where there are too many outcropping layers). In order to avoid a modelling artifact in the SF calculation, we assigned better geomechanical properties (Cretaceous for layers of lower properties) to all elements that are not located in the area of interest i.e. all elements with coarse mesh. In this way, the model is forced to calculate the SF with only the finely meshed elements (Fig. 10). It is more preferable (and recommendable), that a homogeneous mesh be used for the SF calculations (Flac3D manual, Itasca 2019). To adopt a suitable mesh, 2D probabilistic calculations were performed on slope stability test cases: the optimal element size turns out to be 5 m (Ashford and Sitar, 2001; Liu and Glass, 2013.). Therefore, an area of interest was demarcated, the horizontal perimeter of which includes all records of ground movements. This area has, by default, a thickness of 100 m from the topographic surface (aerial and underwater), which can be modified by the presence of the Cretaceous layer within which movements are unlikely (this leads to a lower thickness) and by the position of the base of the mining deposits (the area of interest comprises all the surface formations up to 50 m below the base of the dump units). The elements at the boundaries are cubes having a 50 m edge. Elements between the boundaries and the area of interest are spatially distributed with a geometric ratio. The adopted geometric model thus has finally 11,826,069 elements distributed in Figs. 12, 13.

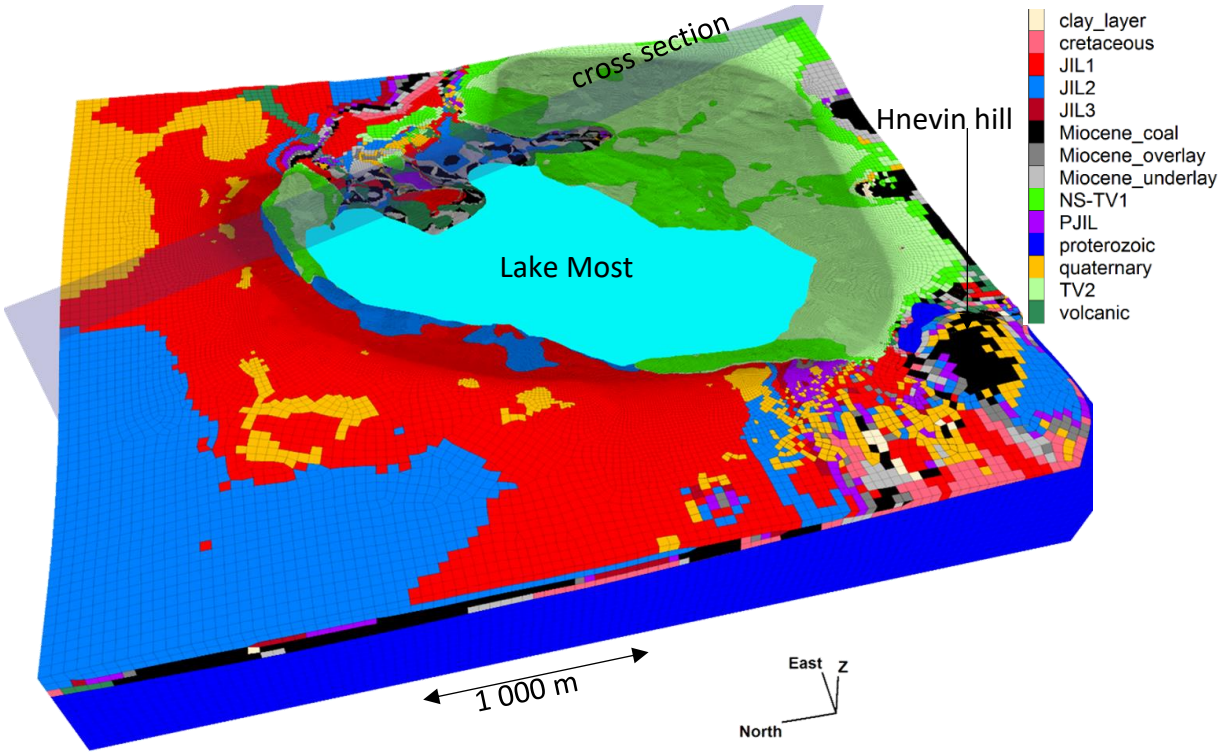

Fig. 12 3D geomechanical model (11 826 069 elements, volume = 15.64 km^3)

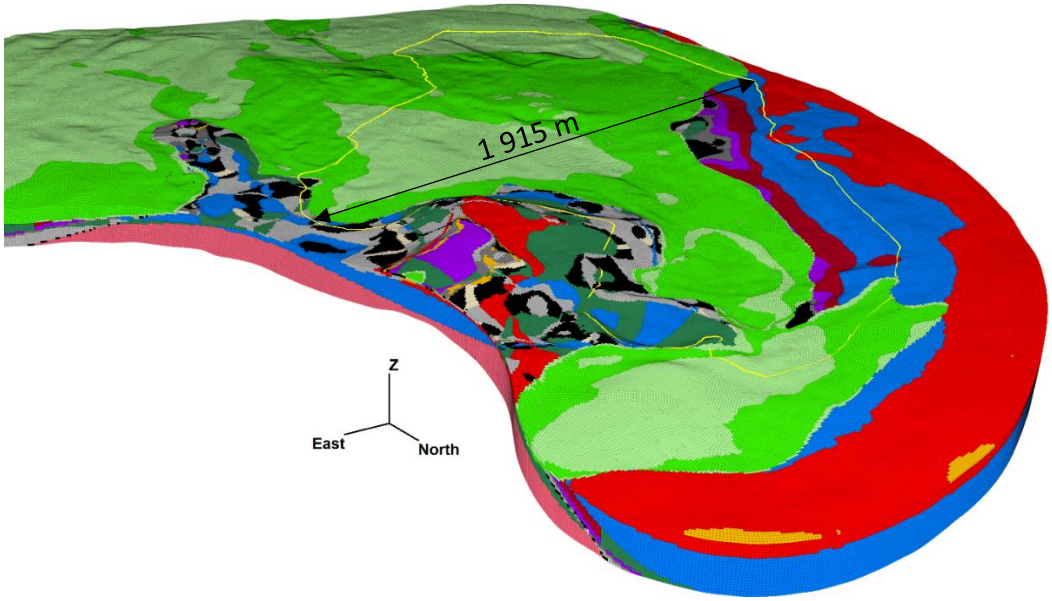

Fig. 13 Refined mesh of the 3D geomechanical model (8 769 185 elements, 74% of total elements, volume = 0.823 km^3)

3.8 Results analysis

3.8.1 NNW-SSE 2D cross section

The SF isovalues maps require 5 days of calculations on a powerful station (32 Xeon E5-2667 v4 cores). Indeed, this type of calculation in increments of SF (increments of 0.05 between SF = 1.2 and 4.0) requires depending on the case more than 150 iterations, knowing that there are 50,000 characteristic response steps for each iteration. This represents about 7,500,000 cycles on a model with 183,807 elements. The results for these 6 calculations are shown in Fig.

14. The calculations (1 to 3) produce the same isovalues of SF (in the range: 1<SF<3). This is because these 3 calculations (without contact layer) differ only in the properties of the dump layers which have large geomechanical properties (higher than the JIL1 unit where the global SF of 2.26 is calculated). On the other hand, calculations including the contact layer (4 to 6) change the stability of all dump units (NS-TV1, TV2 and contact layer). This is explained by the very low properties of the contact layer (Table 3). Areas with SF of 2.75 (NNW) and 2.9 (SSE) without contact layer have a safety factor of between 1.14 and 1.53 at NNW and between 1.5 and 1.6 at SSE when contact layer is present (Fig. 14c, d). There is relatively little difference between scenarios 4 and 5, which suggests that the means properly represent the different distributions of C, E, ϕ and ρ in the dump units. The lowest SF values are obtained in scenario 6 which gives the minimum values for the properties of the dump layers.
A SF equal to 1 indicates the limiting equilibrium state, and this factor should be greater than 1.5 for long-term stability where a 50% safety margin reflects the uncertainties inherent in geological, geomechanical and potential external actions variations, as well as the limitations of computational models. Thus, the safety factor which is equal to 2.26 without the contact layer, is no longer achieved when the contact layer is taken into account (everywhere) at the base of the dump (SF close to 1.5, or even less than 1.5 in some areas at the NNW).
Additionally, the role of the contact layer can be inferred by analysing the fields of deviatoric strain (Stacey et al. 2013) and the stress ratio $(\sigma_1{}^c\text{-}\sigma_3)/(\sigma_1\text{-}\sigma_3)$ at the equilibrium state (before any disturbance caused for the calculation of SF). Indeed, Figs.15, 16 shown that the shear strains are at a maximum in the contact layer and the principal stress ratio is equal to 1. All the elements located above this layer will more easily undergo large strains during the calculation of the SF.

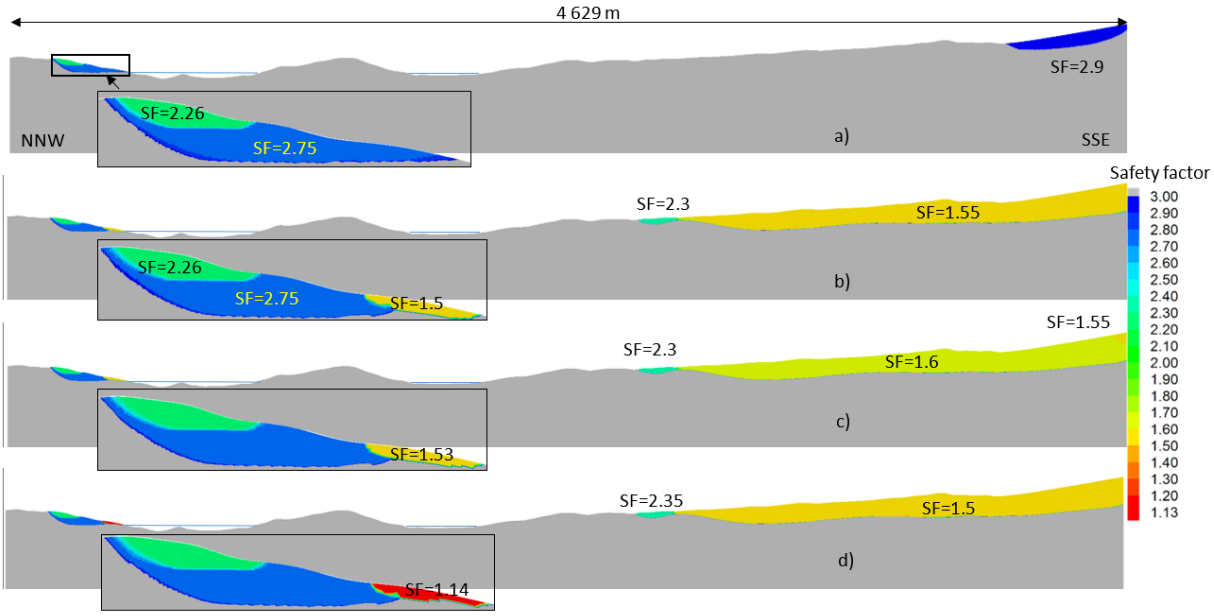

Fig. 14 SF contours for 2D model, a) scenarios 1, 2 & 3; b) scenario 4; c) scenario 5; d) scenario 6

Based on this result, the presence of the contact layer is therefore a strong hypothesis, capable of clearly assessing the stability of the slopes of the Lake Most site. It should be noted that the contact layer was not detected from the CPT campaign measurements. But it is not possible to say that this layer is not present since only 2 boreholes were deeper than the thickness of the dump layers (boreholes P3_9 and P4_14), over an area to be investigated of more than

8 km². The most realistic hypothesis is probably to consider a partial presence of the contact layer. In this case, it is likely that the reality lies between the minorant (with contact layer) and majorant (without contact layer) scenarios. It could then be concluded that the Lake Most site should be stable in the short to medium term.

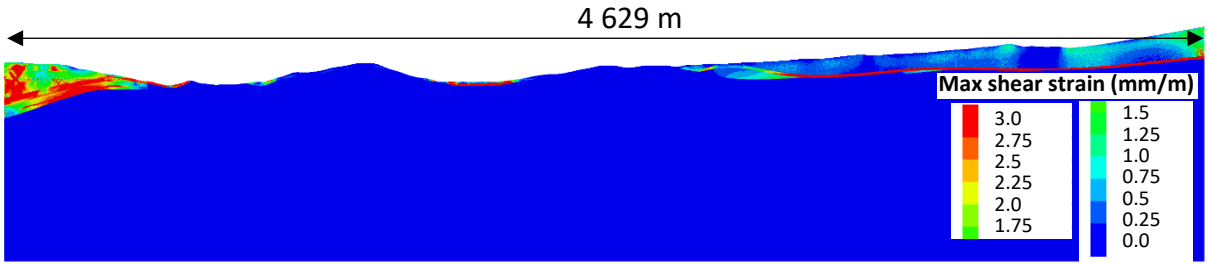

Fig. 15 Maximal shear strain (m/m) at equilibrium

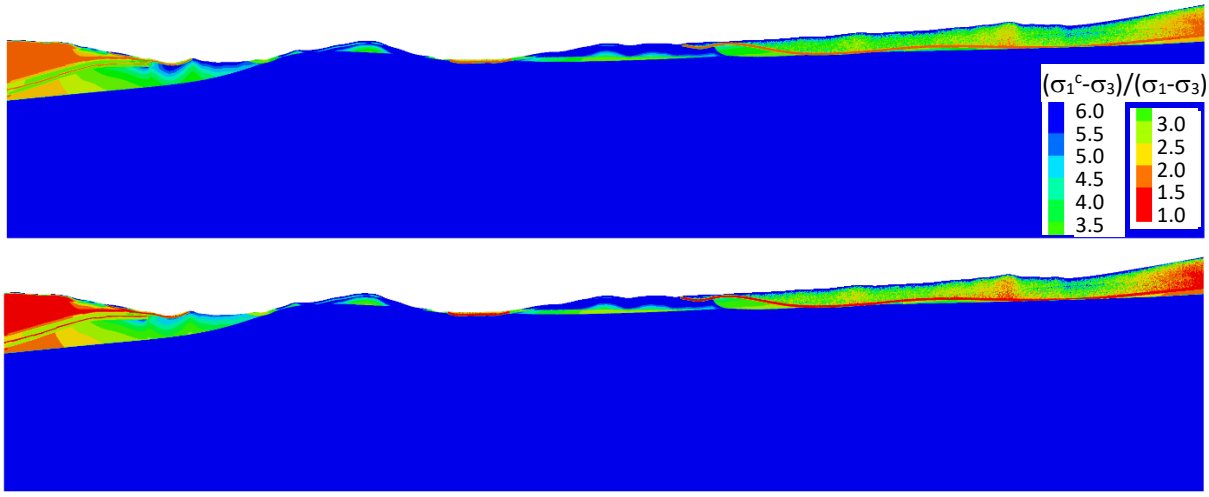

Fig. 16 Ratio $(\sigma_1^c-\sigma_3)/(\sigma_1-\sigma_3)$. a) at equilibrium (top); b) after SF calculation (bottom)

3.8.2 3D model

Four 3D calculations were performed (with or without the presence of the contact layer; with global or local minimum for SF). The global SF minimum is reached on the northern shore of Lake Most, either without contact layer (SF = 2.20) or with contact layer (SF = 1.38). Figs. 17, 18 show the distribution of the local safety factor for the two scenarios.

Comparison of the 3D results with 2D calculation results shows that there is a little difference between 2D and 3D results for the non-contact layer case (2.26 in 2D, 2.2 in 3D) because these SF values are reached in an area with little convexity (easily representable by a 2D cross section). On the other hand, the values of SF for the 2D (1.14) and 3D (1.38) calculations are different for the case with contact layer, corresponding to the conservative effect of geometry in 2D-analyses (Sjoberg et al. 2018).

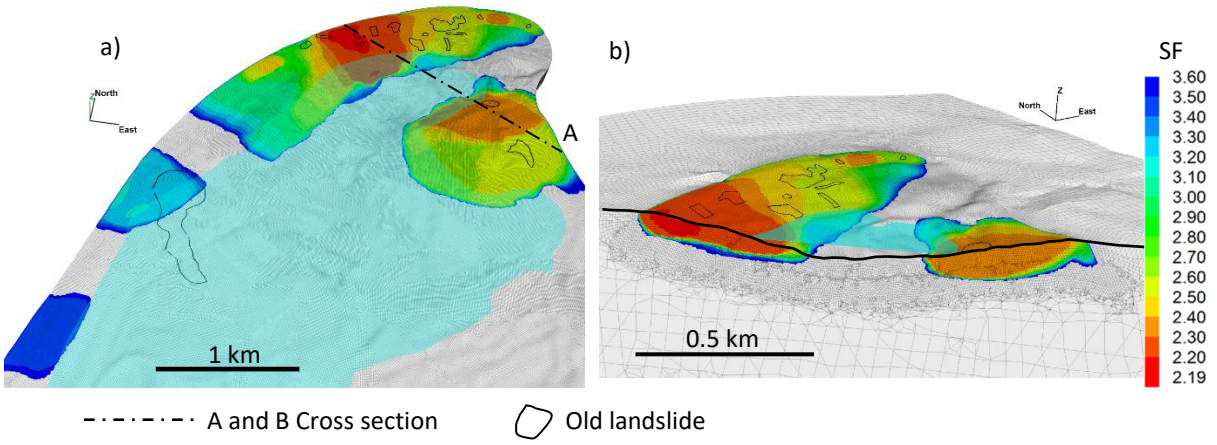

Fig. 17 Safety factor (SF) contour without contact layer. a) 3D view; b) cross section (section A)

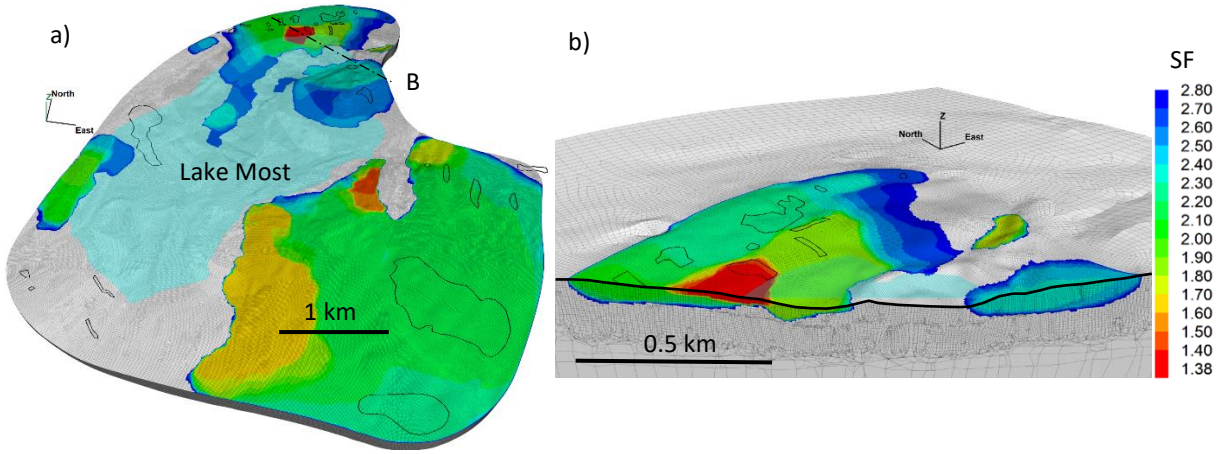

Fig. 18 Safety factor (SF) contour with contact layer, see the contact layer localisation in figure 11 and 19. a) 3D view; b) cross section (section B). Red zones are the critical slope zones (SF < 1.5)

The contours of the old ground movement (creep, landslide, earthflows, mud slides, rockfalls, topple and slope failures) have been added to these figures in order to be able to compare them to the SF isovalues. For the case without contact layer (Fig. 17), there is a very good correlation between the survey of unstable zones of the north and west shores of the lake and the areas where the SF is between 2.2 and 2.7. On the other hand, the (formerly unstable) southern and eastern sectors of the lake have a SF greater than 3.6 (out of SF bracketing range in Flac3D) because they are dump areas (anthropogenic) for which the (current) mechanical characteristics are certainly higher than the surface geological (natural) layers (very present north of the lake) due to the consolidation effect. Those dumps (with their final shapes) have an age varying between 22 and 62 years (in 2021). This long consolidation time can explain an increase in the mechanical properties as a result of the consolidation process. The cross section of Fig. 17b shows that the depths of potential slide surfaces can reach 50 m on the NW side (SF = 2.2, materials = JIL1 until Miocene coal) and 80 m on the SE side (SF = 2.35 to 3.6, materials = JIL1 + JIL2). The shapes of these contours and their minimum SF amplitudes depend on both the topography and the properties of the underlying layers. The irregular shape (far from a classical circular appearance) of the slide surface is explained by the irregular topography and underlying geological layers. However, this is a calculation result that does not consider the dynamic nature of the landslide phenomenon: it is very likely that the skew surface would be more homogeneous for a real case of slope failure.

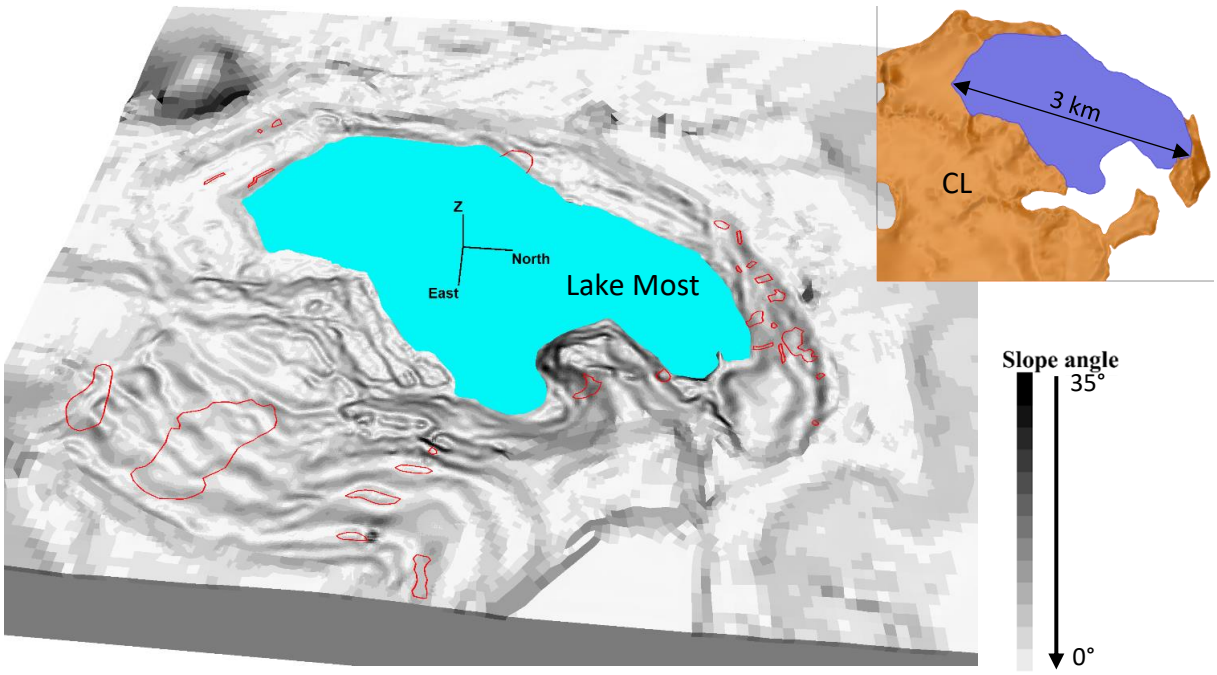

Fig. 19 Slope angle contour, localisation of landslides (red curves) and contact layer (CL)

For the case with a contact layer (Fig. 18), there is a very good correlation between the survey of unstable areas of the north and east shores of the lake and the areas where the SF is between 1.38 and 2.6. On the other hand, the southern (formerly unstable) areas of the lake have a SF greater than 3.6 because they are the weakest sloped areas of the lake's shores (Fig. 18). The western sector does not appear in Fig. 18 due to the change in the SF bracketing interval (limited here to 2.8 to decrease the calculation times). But as it is a sector without dump (Fig. 7), there is no contact layer in this area: the isovalues of SF are therefore the same as in Fig. 17 (3.2<SF<3.6).

3.8.3 Results discussion

The entire eastern part of the Lake Most is influenced by the weak properties of the contact layer (Fig. 18). But since the southern part of the lake is a low-sloped sector (Fig. 19), SF varies essentially between 1.4 and 2.4.

The Fig. 18 shows that the depths of potentially unstable zones can reach 50 m on the NW side (SF = 2.2, materials = JIL1 until Miocene coal and contact layer) and 60 m on the SE side (SF = 2.35 to 2.8, materials = JIL1 + JIL2). These depths are comparable to the case without contact layer. This is explained by the fact that the geological layer under the dump is sufficiently resistant (Table 1) not to be part of the slope failure zones. The fact that the eastern zones that have undergone ground movements in the past cannot be correlated with a low SF (the calculation of which includes a contact layer) shows that the initial properties of the dump layers must have been much lower than those measured recently (in 2020). Indeed, the 6 landslide zones to the east have a SF varying between 1.8 and 2.3, which is considered stable based on the stability analysis recommendations. It is recalled that the extraction of coal from the last mine in the sector (Lezaky or Most-Kopisty) was completed in 1999, but the dumping process (as a final reclamation) continued until 2002. Fig. 2 shows the dates for the 3 main groups of dumps around Lake Most while Fig. 7 shows the dates on which the landslides occurred. The joint analysis of these 2 figures shows that the mass movements in the north are recent, that they occurred between 9 years and 22 years after the final form of the dump. On the other

hand, all other mass movements are old. Those in the west (DLM dump) occurred at least 7 years before the start of work on the dump. It is the same for the mass movements in the east (Strimice dump). Landslides were partially excavated or buried by younger dump layers. This implies that the search for a spatial correlation between a low SF and landslides only concerns the northern sector of the lake (Konobrze dump).

The consolidation of the dumps depends on the height of the dumps and varies between a few years to more than 20 years. The Konobrze dump has been under consolidation process for 9 to 22 years. The modification of the hydraulic conditions can impact the consolidation process and increase the settlement and ground movement of the dumps (Wayne et al. 2008).

For the computation without contact layer, it is reasonable to conclude that the site is stable since the global minimum SF is equal to 2.2. On the other hand, for the calculation with contact layer, 2 sectors (north and east of Lake Most) present an SF less than 1.5 corresponding to critical potential unstable zones. These 2 calculations correspond to the lower and upper limits of the stability calculation. The real situation is undoubtedly between these 2 limits. As it would be very long and very expensive to drill numerous boreholes in order to map the contact layer, it would be more judicious to check it only on these 2 sectors. If the test turns out to be negative (no contact layer), we will be able to assess the medium-term stability of the site with greater certainty.

4 CONCLUSIONS

The main objective is to assess the slope stability of open-pit lake using a large-scale 3D numerical model. To achieve this objective, a reliability methodology for assessing the long-term stability of open-pit lake was developed. A large-scale numerical model (multi-km) of the lake was generated using Flac3D and was applied on Lake Most (Czech Republic). This model was built, based on the site observations, large scale LiDAR data and geotechnical data. The model incorporates the complex geology of the mine and the dumps as well as the surface of the water table interpolated from 93 piezometric levels.

The expected morphological vulnerability of the area surrounding the lake concerns zones with flush layers with weak geomechanical properties (layers JIL1 and PJIL) or which are directly above the contact layer.

The results were analysed by calculating a global and local safety factor using strength reduction method. The results demonstrated the reliability of the methodology in combining the geometric, geological and hydraulic models to create a large-scale numerical model, and to identify local potentially instable zones. The 3D calculations give results compatible with the 2D cross section. The global 3D SF is located on the north bank of Lake Most at the location where most slope failure stabilization operations took place in the past. The calculation of 3D SF has shown a very good correlation between the lowest SF and the ground movement observations noted by the Czech authorities (landslide, earthflow, mud slide, rockfall, slope failure).

The numerical modelling highlighted the role of a weak contact layer. It should be noted that the contact layer was not detected from the CPT campaign measurements. But neither the absence nor the presence of the contact layer can be confirmed because only 2 profiles are deeper than the dump units in an area of more than 8 km² to be investigated. The hypothesis of the presence of a very weak contact layer (at the bottom of dump bodies) is therefore a

strong hypothesis, capable of clearly assessing the stability of the Lake Most slopes. The most realistic hypothesis is probably to consider a partial presence of the contact layer. These new calculations could show whether the reality lies between the minorant (with contact layer) and majorant (without contact layer) scenarios. For this study, it can therefore be concluded that the Lake Most site should be stable in the short to medium term.

The application of this methodology to the case of Lake Most therefore constitutes a validated method for carrying out slope stability analysis in very complex geomechanical and geotechnical post-mine sites.

Author contribution Vincent Renaud: geometrical, geological and geotechnical models, code writing, data processing, statistical analysis, bibliographic research, writing original draft. Marwan Al Heib: writing review, bibliographic research, results analysis. Jan Burda: collecting data, map production, bibliographic research, writing review. All authors have read and agreed to the published version of the manuscript.

Funding This work has received funding from the European Union's Research Fund for Coal and Steel (RFCS). under the project "Risk Assessment of final Pits during Flooding (RAFF)". No 847299.

Declarations

Conflict of interest The authors declare no competing interests

5 REFERENCES

1. Alejano LR, Ferrero AM, Oyanguren PR, Fernandes MIA (2011) Comparison of limit equilibrium, numerical and physical models of wall slope stability. Int J Rock Mech Min Sci 48: 16-26.
2. Apostu IM, Lazar M, Faur F (2020) A Model to Evaluate the Flooding Opportunity and Sustainable Use of Former Open-Pits. Sustainability 2020, 12, 9275. https://doi.org/10.3390/su12219275.
3. Atkinson LC (2001) The Role and Mitigation of Groundwater in Slope Stability. Slope Stability in B.C., Canada.
4. Ashford SA, Sitar N (2001) Effect of element size on the static finite element analysis of steep slopes. Int J Numer Anal Methods Geomech 25(14): 1361-1376.
5. Bishop AW (1955) The use of the slip circle in the stability analysis of slopes. Geotechnique 5: 7-17.
6. Bye A, Bell F (2001) Stability assessment and slope design at Sandsloot open pit, South Africa. Int J Rock Mech Min Sci 38(3): 449-466. https://doi.org/10.1016/s1365-1609(01)00014-4
7. Cala M, Polak K (2012) Utilization of surface and groundwater for post-mining open pits reclamation in lignite mining. AGH J Min Geoengineering 36(10): 83-90.
8. Chen RH, Chameau JL (1982) Three-dimensional limit equilibrium analysis of slopes. Geotechnique 32: 31-40.
9. Cherubini C (2000) Reliability evaluation of shallow foundation bearing capacity on c′ −φ′ soils. Can Geotech J 37(1): 264-269.

10. Caudal P, Grenon M, Turmel D, Locat J (2017) Analysis of a Large Rock Slope Failure on the East Wall of the LAB Chrysotile Mine in Canada: LiDAR Monitoring and Displacement Analyses. Rock Mech Rock Eng 50: 807-824. https://10.1007/s00603-016-1145-3
11. Dawson EM, Roth WH, Drescher A (1999) Slope stability analysis by strength reduction. Geotechnique 49(6): 835-840. https://doi.org/10.1680/geot.1999.49.6.835
12. Fredlund DG, Krahn J (1977) Comparison of slope stability methods of analysis. Can Geotech J 14(3): 429-439.
13. Gallwey J, Eyre M, Tonkins M, Coggan J (2019) Bringing Lunar LiDAR Back Down to Earth: Mapping Our Industrial Heritage through Deep Transfer Learning, Remote Sens 11(1994): 1-22. https://doi.org/10.3390/rs11171994.
14. Geller W, Schultze M, Kleinmann B, Wolkersdorfer C (2013) Acidic Pit Lakes: The Legacy of Coal and Metal Surface Mines. Series: Environ Sci Eng. Berlin: Springer.
15. Goodman RE (1989) Introduction to rock mechanics. New York, United States: Wiley.
16. Griffiths DV, Lane PA (1999) Slope stability analysis by finite elements. Geotechnique 49(3): 387-403. https://doi.org/10.1680/geot.1999.49.3.387
17. Hoek E (2000) Rock engineering. Course Notes, E. Hoek Consulting Engineer Inc., North Vancouver, Canada.
18. Hoek E, Bray JW (1981) Rock slope engineering. London, United Kingdom: Institution of Mining and Metallurgy.
19. Itasca (2019) FLAC3D (Fast Lagrangian Analysis of Continua in Three Dimensions) version 7.0, User's Guide and Command Reference. Itasca Consulting Group Inc. Minneapolis, USA.
20. Jaeger JC (1971) Friction of rocks and stability of rock slopes. Geotechnique 21(2): 97-134. https://doi.org/10.1680/geot.1971.21.2.97
21. Johnstone A (2018) Coal mine pit lakes: a viable mine closure option? Mining review Africa. https://www.miningreview.com/coal/coal-mine-pit-lakes-a-viable-mine-closure-option/
22. Kulhawy FH, Mayne PW (1990) Manual on estimating soil properties for foundation design, Report EL-6800 Electric Power Research Institute, EPRI.
23. Lazar M, Faur F, Apostu IM (2020) Influence of the flooding speed of former lignite open pits on the stability of final slopes. MATEC Web of Conferences 305(00040). https://doi.org/10.1051/matecconf/202030500040
24. Liu Y, Glass G (2013) Effects of mesh density on finite element analysis. SAE international. SEA Technical paper. https://doi.org/10.4271/2013-01-1375.
25. Lumb P (1970) Safety factors and probability distribution of soil strength. Can Geotech J 7(3): 225-242.
26. Matsui T, San KC (1992) Finite element slope stability analysis by shear strength reduction technique. Soils Found 32(1): 59-70. https://doi.org/10.3208/sandf1972.32.59.
27. Mayne PW (2006) In situ test calibrations for evaluating soil parameters. Proc, Characterization and Engineering Properties of Natural Soils II, Singapore.
28. McCullough CD, Schultze M, Vandenberg J (2020) Realizing Beneficial end uses from abandoned pit lakes. Minerals 10(2): 133. https://doi.org/10.3390/min10020133. (Mine Lakes Consulting, minelakes consulting).
29. Meng J, Mattsson H, Laue J (2021) Three-dimensional slope stability predictions using artificial neural networks. Int J Numer Anal Methods Geomech 45(13): 1988-2000.
30. Merrien-Soukatchoff V, Omraci K (2000) Determination of boundary conditions for a slope stability calculation. Rev Fr Geotech 92: 31-39. https://doi.org /10.1051/geotech/2000092031.

31. Mikroutsikos A, Theocharis AI, Koukouzas NC, Zevgolis IE (2021) Slope stability of deep surface coal mines in the presence of a weak zone. Geomech Geophys Geo-Energy Geo-Resour 7(66). https://doi.org/10.1007/s40948-021-00265-2.
32. Motaghedi H, Eslami A (2014) Analytical Approach for determination of soil shear strength parameters from CPT and CPTu data. Arab J Sci Eng 39: 4363-4376.
33. Nikolic T, Spago A, Spago S, Sahinagic-Isovic M, Ademovic N (2019) The slope stability around an artificial lake Jablanica, with landslide sample project recovery in Donje Paprasko – Jablanica. Uljarevic M, Zekan S, Ibrahimovic Dz (eds.) Proceedings of the 4th Regional Symposium on Landslides in the Adriatic Balkan Region, Sarajevo, Bosnia and Herzegovina.
34. Oggeri C, Fenoglio TM, Godio A, Vinai R (2019) Overburden management in open pits: options and limits in large limestone quarries. Int J Min Sci 29: 217-228.
35. Qiujing P, Jingshu X, Dias D (2017) Three-Dimensional Stability of a Slope Subjected to Seepage Forces. Int J Geomech 17(8): 1-9.
36. Redondo-Vega JM, Melon-Nava A, Peña-Pérez SA et al. (2021) Coal pit lakes in abandoned mining areas in León (NW Spain): characteristics and geoecological significance. Environ Earth Sci 80(792). https://doi.org/10.1007/s12665-021-10037-6.
37. Robertson PK, Campanella RG (1983) Interpretation of cone penetration tests – Part I (sand). Can Geotech J 20(4): 718-733.
38. Robertson PK, Campanella RG, Gillespie D, Greig J (1986) Use of Piezometer Cone data. In-Situ'86 Use of In-situ testing in Geotechnical Engineering, GSP 6 , ASCE, Reston, VA, Specialty Publication, SM 92, pp 1263-1280.
39. Robertson PK (1990) Soil classification using the cone penetration test. Can Geotech J 27(1): 151-158
40. Schneider J, Randolph M, Mayne PW, Ramsey NR (2008) Analysis of Factors Influencing Soil Classification Using Normalized Piezocone Tip Resistance and Pore Pressure Parameters. J Geotech Geoenviron Eng 134(11):1569-1586
41. Schultze M, Pokrandt KH, Hille W (2010) Pit lakes of the Central German lignite mining district: Creation, morphometry and water quality aspects. Limnologica 40(2): 148-155. https://doi.org/10.1016/j.limno.2009.11.006.
42. Schultze M, Hemm M, Geller W, Benthaus FC (2013) Pit Lakes in Germany: Hydrography, Water Chemistry, and Management. In Acid Pit Lakes: The Legacy of Coal and Metal Surface Mining, Geller W, Schultze M, Kleinmann R and Wolkersdorfer C ed., Heidelberg, Germany, Springer. 265-291.
43. Sjöberg J, Alvarez DL, Gomez P, Marklund PI, Suikki S (2018) Analysis of large-scale pit slope stability - The Aitik Mine revisited. International symposium in slope stability in open pit mining and civil engineering at the XIV international congress for energy and resource mining in Seville.
44. Soren K, Budi G, Sen P (2014) Stability analysis of open pit slope by finite difference method. Int J Eng Res Technol 3(5): 326-334. https://doi.org/10.15623/ijret.2014.0305062
45. Stacey TR, Xianbin Y, Armstrong R, Keyter GJ (2003) New slope stability considerations for deep open pit mines. J S Afr Inst Min Metall 103(6): 373-389. doi.org/10.1016/j.ijmst.2018.06.011 2095-2686, Open Access.
46. Steiakakis E, Thalassinakis J, Agioutantis Z, Galetakis M (2016) Failure process of the external waste dump of a lignite mine using finite element method (FEM). 13th International Symposium Continuous Surface Mining ISCSM 2016, Belgrade, Serbia, 11-14 September 2016.

47. Terzaghi K (1925) Earthwork mechanics based on soil physics. Deuticke, Vienna, Austria.
48. Theocharis AI, Zevgolis IE & Koukouzas NC (2021) A comprehensive geotechnical characterisation of overburden material from lignite mine excavations. Geomech Geophys Geo-energ Geo-resour 7(30). https://doi.org/10.1007/s40948-021-00230-z.
49. Vanneschi C, Eyre M, Burda J, Zizka L, Francioni M, Coggan JS (2018) Investigation of landslide failure mechanisms adjacent to lignite mining operations in North Bohemia (Czech Republic) through a limit equilibrium/finite element modelling approach. Geomorphology 320: 142-153, https://doi.org/10.1016/j.geomorph.2018.08.006.
50. Vinzelberg G, Dahmen D (2014) The Inden Residual Lake and the Federal Autobahn A44n—Geotechnical Requirements to Be Met by Large-Scale Structures in the Rhenish Lignite Mining Area. In Proceedings of the 12th International Symposium Continuous Surface Mining—Aachen 2014; Springer: Cham, Switzerland; pp. 91-100.
51. Wayne A, Karem, Craig S, Lee PE (2008) Settlement evaluation of end dumped coal mine spoil fill. National Meeting of the American Society of Mining and Reclamation, Richmond, VA.
52. Wolff TH (1985) Analysis and design of embankment dam slopes: a probabilistic approach. PhD thesis. West Lafayette, Indiana, US: Purdue University.
53. Wyllie DC, Mah CW (2017) Rock slope engineering. London, United Kingdom: Spon Press. https://doi.org/10.4324/9780203499085.
54. Yang T, Yeung MR, Yang B, Liu Y, Yang Y (2016) Three-dimensional stability of landslides based on local safety factor. J Mt Sci 13(9): 1515-1526.
55. Yongtao Y, Yang X, Hong Z, Zhijun L (2021) Investigation of rock slope stability using a 3D nonlinear strength-reduction numerical manifold method. Eng Geol 292, 15 p. https://doi.org/10.1016/j.enggeo.2021.106285.
56. Yücemen MS, Tang WH, Ang AHS (1973) A probabilistic study on safety and design of earth slopes. Urbana, US: Civil Engineering Studies, Structural research Series 402, University of Illinois.
57. Zienkiewicz OC, Humpheson C, Lewis RW (1975) Associated and non-associated visco-plasticity and plasticity in soil mechanics. Geotechnique 25(4): 671-689.
58. Zienkiewicz OC, Taylor RL (2000) The Finite Element Method, 5th ed. Butterworth-Heinemann, Oxford.
59. Zizka L, Burda J (2021) Post Exploitation Lakes. In Zpravodaj Hnede Uhli; Brown Coal Research Institute: Budovatelu, Czech Republic; pp. 11-46.